# Dynamic behavior of simple magnetic hole systems

G. Helgesen
*Department of Physics, University of Oslo, N-316 Oslo 3, Norway*

P. Pieranski
*Institute of Molecular Physics, Polish Academy of Sciences, 60-179 Poznan, Poland*

A.T. Skjeltorp
*Institute for Energy Technology, N-2007 Kjeller, Norway*
(Received 22 June 1990)

Experiments on a system of two magnetic holes (nonmagnetic microspheres in ferrofluid) subject to a rotating magnetic field show various types of behavior depending on the driving frequency. For two spheres (holes) mechanically bound together the stable rotation mode at low frequencies is replaced above a critical frequency by a mode with alternating rotation directions. This is described by simple nonlinear equations, and simulations show good quantitative agreement with the experiments. For two free spheres not bound together one observes a transition to a mode in which the spheres undergo both angular and radial motion around the center of mass of the system. Depending on the frequency and the anisotropy of the rotating magnetic field the motion passes through a sequence of states with sphere rotation mode-locked to the driving frequency at different ratios in good qualitative agreement with simulations. Adding a constant magnetic field normal to the plane causes the minimum sphere separation to increase from contact to a finite value. At high frequencies the spheres are influenced by an effective magnetic potential, giving rise to a static particle separation proportional to the normal component of the field.

## I. INTRODUCTION

The term *magnetic hole* has been used to denote a nonmagnetic particle immersed in a ferrofluid.[1,2] The interesting properties of such systems have been studied for some time. The crystallization and melting of monolayers of these magnetic holes in external fields have been observed experimentally, and it has been predicted that there should be phase transitions between various static two-dimensional (2D) and quasi-2D phases depending on the layer thickness.[3] On the other hand, the dynamic behavior of such systems is not well known even though there have been some theoretical calculations for the motion and orientation of similar systems consisting of fine ferromagnetic particles in a viscous medium.[4,5]

The understanding of the dynamics as well as the statics of these systems should be important in connection with ferrofluid applications[6,7] and for use of magnetic microspheres in medicine.[8] From the theoretical point of view the magnetic hole systems offer the possibilities of observing a wide range of nonlinear dynamic phenomena and collective processes, as they are easy to produce and to manipulate. A simplifying feature with magnetic holes is that their magnetic moments are collinear with an external field at any field strength. This is in contrast to fine magnetic particles for which intrinsic anisotropies, domains, etc. complicate the theoretical treatment of the dynamic and static properties of particle assemblies.

## II. EXPERIMENT

Our experimental system consisted of a thin layer (typically 50–100 $\mu$m) of kerosene-based ferrofluid[9] confined between two glass plates. Highly monodisperse polystyrene spheres[10] in size range 10-100 $\mu$m were dispersed in the fluid. The spheres are so large that they may be stored dry and dispersed directly into the ferrofluid. Moreover, since the spheres are hydrophobic they enter easily the bulk of the fluid. The separation between the plates was adjusted evenly by using either somewhat larger spheres (50–100%) as spacers or using a thin wire along the edges. The cell was sealed along the edges and was placed in a magnetic field produced by three orthogonal pairs of coils, along the $x$, $y$, and $z$ directions. The microscope used to observe the spheres was connected to a video camera, a videotape recorder, and a computer with a digitizing card for numerical analysis of the video pictures.

A magnetic liquid consists of a colloidal suspension of monodomain ferromagnetic particles (e.g., magnetite) of typical size 100 Å coated with surfactants to prevent aggregation and dispersed in water or an organic liquid. The Brownian motions of the particles prevent sedimentation. In an external magnetic field the ferrofluid particles will partly align with the field and thus the ferrofluid is perfectly paramagnetic. Since the diameter of the nonmagnetic polystyrene spheres we used was several

 

orders of magnitude larger than the ferrofluid particles, the spheres (holes) moved in a homogeneous, magnetic background. The particle nature of the ferrofluid may thus be neglected in the present case. The interaction between the dispersed nonmagnetic spheres is of dipole-dipole type. It should also be noted that the spheres were so large that their Brownian motions had no influence. (For spheres smaller than 2 $\mu$m diameter this has to be taken into consideration.) In the presence of a constant $H$ field in the $xy$ plane (sample plane) the magnetic holes line up in chains oriented along the field. There is an apparent repulsive dipole interaction between the chains forcing them to separate as far as possible. With only a constant magnetic field normal to the sample plane (along the $z$ axis), the magnetic holes repel each other and locally produce a triangular lattice with lattice constant comparable to the sphere diameter, i.e., 10–100 $\mu$m typically. It is possible to "anneal" the lattice, e.g., by using an oscillating field, and to obtain a perfect triangular lattice on long length scales too (>1 cm).

The regular structures observed in stationary fields are destroyed when the direction of the field is changing, as in a rotating field. The many-body modes of motion which appear in this case are in general very complex, but in some special cases their spatiotemporal structure becomes quite simple and clear. To gain insight into the problem, we performed a series of experiments on samples containing only a few spheres. In this article, we will consider the simplest case with only two spheres (magnetic holes). The three-sphere case is much more complicated and has not yet been thoroughly investigated.

The experimental situation for two magnetic holes in an $H$ field rotating in the $xy$ plane is shown in Fig. 1. The components of the field are $H_{0X}\sin(\omega_H t)$ and $H_{0Y}\sin(\omega_H t+\pi/2)$ where $\omega_H$ is the angular frequency of the rotation. Both circularly polarized ($r = H_{0Y}/H_{0X} = 1$) and elliptically polarized fields ($r < 1$) were used. The frequencies of the modes of motion for the spheres were low (<1 Hz) and were measured manually by using a stopwatch. Two distinctly different physical realizations were employed: In case (i), the spheres were bound together permanently[11] so that there was only one degree of freedom left for their motion, the angular rotation. The system was then similar to a single anisotropic particle in a rotating field. In case (ii), the spheres were free to separate, and this produced different and more complex modes of motion. These two cases will thus be discussed separately below.

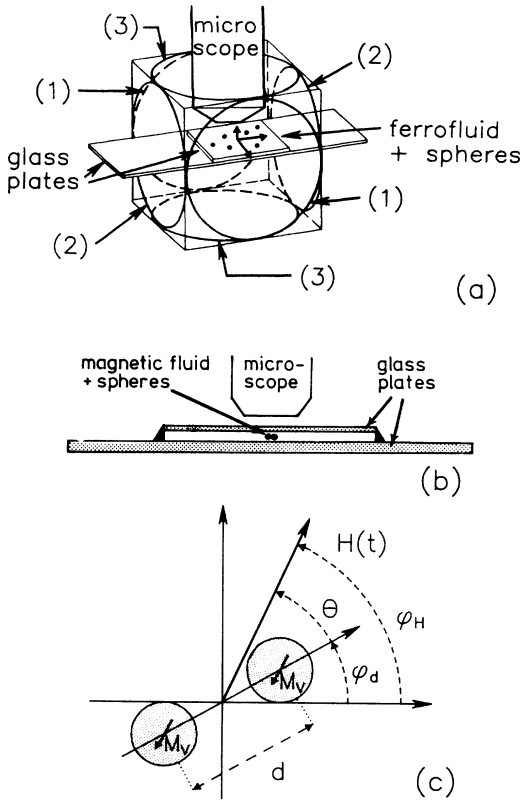


FIG. 1. (a) Experimental setup, showing the three orthogonal pairs of coils labeled (1), (2), and (3). (b) Side view of experimental setup (without coils). (c) Top view, coordinate system for two magnetic holes rotating in the plane between the glass plates in (b).

### A. Case (i): Bound spheres

For circularly polarized fields ($r$=1) there are two distinctly different steady-state modes of motion.[12] For low frequencies $\omega_H$ of the rotating magnetic field, the bound pair rotates uniformly and is phase-locked to the field. This mode is denoted by $M_1^c$ (the superscript $c$ in the mode notation indicates a circular rotating field). It occurs below a well-defined angular frequency, $\omega_C$, of the rotating field. (Typically, $\omega_C/2\pi = 0.3 - 0.5$ Hz

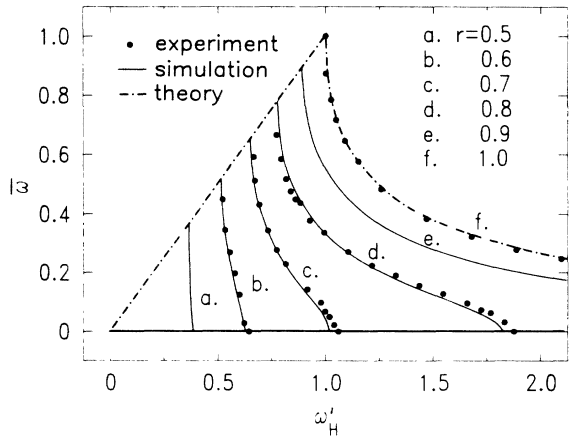


FIG. 2. Plots of the average angular frequency $\overline{\omega}$ for various amplitude ratios $r = H_{0Y}/H_{0X}$ of the rotating magnetic field vs $H$-field angular frequency $\omega'_H$. The dash-dotted curve for $r$=1 (curve $f$) is the exact analytical solution given by Eq. (14). The solid curves represent simulated results and the dots experimental results. The intersections of the solid curves (a)-(e) with the dash-dotted line to the left ($\overline{\omega} = \omega'_H$) represent the critical frequencies $\omega_1$ in Fig. 5, whereas the intersections with the horizontal solid line ($\overline{\omega} = 0$) represent the critical frequencies $\omega_2$ in Fig. 6.

in most cases.) Above $\omega_C$, the motion is no longer uniform. Instead, the pair goes through a periodic sequence of forward and backward rotations (mode $M_2^c$). For $\omega_H$ just above $\omega_C$, the forward rotations last much longer than the backward ones. As $\omega_H$ increases, they become more frequent and comparable in length. On average, the bound pair rotates in the same direction as the rotating field, but the average angular frequency $\overline{\omega}$ of this motion goes to zero as $\omega_H \to \infty$. This average behavior is shown in Fig. 2 where all frequencies are normalized relative to $\omega_C$ ($\omega'_H = \omega_H/\omega_C$). It was observed that this critical frequency, which separates the modes $M_1^c$ and $M_2^c$, is proportional to the square of the magnitude of the rotating field.

Using different amplitudes of the two components $H_{0X}$ and $H_{0Y}$ of the rotating field (elliptical field) the transition from the phase-locked state (denoted by $M_1$) to the forward-backward rotation mode $M_2$ now occurs at a lower frequency than $\omega_C$. The $M_1$ mode may be considered as a modulated version of the $M_1^c$ mode with the angular velocity of rotation oscillating at a frequency $2\omega_H$ with small amplitude around the average value $\omega_H$. Similarily, the $M_2$ mode can be seen as a modulation of the $M_2^c$ mode.

### B. Case (ii): Free spheres

When the spheres are not bound together, the system has an additional radial degree of freedom, and the motion becomes more complex. The phase-locked $M_1^c$ mode, however, remains unchanged. At $\omega_C$ it transforms into a new mode $M_4^c$. The angular behavior (oscillations) of the system in this mode is similar to the $M_2^c$ mode, but an additional radial oscillation takes place each time the axis between the spheres rotates opposite to the field. The spheres thus move in antiphase in loops around the fixed mass center of the system. The number of loops increases with increasing frequency of the driving field.

For the anisotropic case $H_{0X} \neq H_{0Y}$ ( $r < 1$ ) the loops are no longer even but vary according to the magnitude of the magnetic field. The most important difference between the bound and free pair cases is that in the latter case we observe locking to the external frequency for other ratios than the simple $\overline{\omega}:\omega_H = 1:1$ $M_1^c$ mode observed for bound spheres. For certain intervals of $\omega_H$, the rotation of the pair locks to the field in ratios $\overline{\omega} : \omega_H = 1:2$, 1:4, 1:6, 2:3, etc. as will be shown later in the simulation part of this paper.

## III. PHYSICAL MODEL

Let us consider a system of two equal nonmagnetic spheres with diameters $a$ ($a = 10-100$ $\mu$m) placed inside a thin layer of magnetic fluid confined between two glass plates with spacing typically twice the diameter of the spheres. In an external magnetic field, the holes carry an apparent magnetic moment $\mathbf{M}_V = -V\chi_{\text{eff}}\mathbf{H}$ where $V = \pi a^3/6$ is the sphere volume and $\chi_{\text{eff}}$ is the effective volume susceptibility of the ferrofluid.[1] These apparent magnetic moments $\mathbf{M}_V$ carried by each magnetic hole are equal and always parallel to the magnetic field, but opposite to its direction. This is a magnetic analog of Archimedes's principle. Figure 1(c) shows the situation when two spheres are placed in an external rotating field $\mathbf{H}(t)$ which at time $t$ makes an angle $\phi_H$ with the $x$ axis. We assume that the line through the centers of the spheres, which are separated by a distance $d \geq a$, makes an angle $\phi_d$ with the $x$ axis. The interaction energy between the spheres is given to first order[13] by the dipolar term

$$U = M_V^2[1 - 3\cos^2(\phi_H - \phi_d)]/d^3 \ . \tag{1}$$

When the magnetic field is rotating with angular velocity $\omega_H$, we obtain

$$M_V^2 = V^2\chi_{\text{eff}}^2 H_0^2(\cos^2\omega_H t + r^2\sin^2\omega_H t) \ , \tag{2}$$

with $r = H_{0Y}/H_{0X}$, $H_0 = H_{0X}$ and

$$\tan\phi_H = r\tan\omega_H t \ . \tag{3}$$

The radial magnetic force $F_d^H$ acting on each of the spheres is

$$F_d^H = -\frac{\partial U}{\partial d} = 3M_V^2[1 - 3\cos^2(\phi_H - \phi_d)]/d^4 \ , \tag{4}$$

and the magnetic torque $G_\phi^H$ acting on the pair is

$$G_\phi^H = -\frac{\partial U}{\partial \phi_d} = 3M_V^2\sin[2(\phi_H - \phi_d)]/d^3 \ . \tag{5}$$

Assuming a simple Stokes law for the viscous force $F^\eta$ acting on the spheres, the radial and angular components, $F_d^\eta$ and $F_\phi^\eta$, are

$$F_d^\eta = -3\pi\eta a(\tfrac{1}{2}\dot{d}) \tag{6}$$

and

$$F_\phi^\eta = -3\pi\eta a\left(\frac{d}{2}\dot{\phi}_d\right) \ , \tag{7}$$

respectively, where $\eta$ is the ferrofluid viscosity.

In equilibrium, $F_d^H + F_d^\eta = 0$. Since the magnetic torque on each of the spheres is $\frac{1}{2}G_\phi^H$, the equilibrium condition for the torques about the center of rotation can be written $\frac{1}{2}G_\phi^H + \frac{d}{2}F_\phi^\eta = 0$. We introduce new dimensionless variables for distance $D = d/a$, time $\tau = \omega_C t$, angular frequency $\omega'_H = \omega_H/\omega_C$, and field $\mathbf{h} = \mathbf{H}/H_0$. The constant $\omega_C$ is given by

$$\omega_C = \pi H_0^2\chi_{\text{eff}}^2/18\eta \ , \tag{8}$$

which corresponds to the experimentally observed critical angular frequency described above.

Thus the dimensionless equations of motion for a pair of holes are

$$\frac{dD}{d\tau} = h^2[1 - 3\cos^2(\phi_H - \phi_d)]/D^4 \tag{9}$$

and

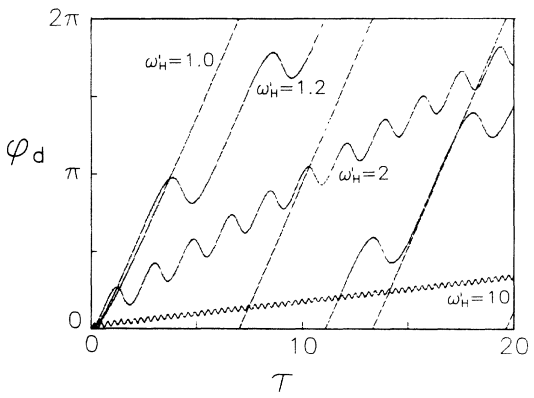


FIG. 3. The angular position $\phi_d$ vs time $\tau$ for two bound spheres in a circular symmetric rotating magnetic field for different field angular frequencies $\omega'_H$. The initial conditions for all simulations were $\phi_d(\tau = 0) = \phi_H(\tau = 0) = 0$.

$$\frac{d\phi_d}{d\tau} = h^2 \sin[2(\phi_H - \phi_d)]/D^5 \ . \tag{10}$$

The magnitude of the dimensionless magnetic field **h** is given by

$$h^2 = \cos^2(\omega'_H\tau) + r^2 \sin^2(\omega'_H\tau) \ . \tag{11}$$

In the reasoning above, we have neglected the inertia term $I\ddot{\phi}_d$ since the moment of inertia $I$ is small and the viscosity of the ferrofluid is high (strong damping, Reynold's number $R \approx 10^{-5}$). Using Eqs. (9)–(11) above we have performed numerical simulations on the system using a fourth-order Runge-Kutta algorithm. The results of these simulations are presented in Figs. 2–4. Due to the strong damping of the system, the initial transients were always relatively short except when $\omega'_H$ was close to the critical frequencies as discussed below.

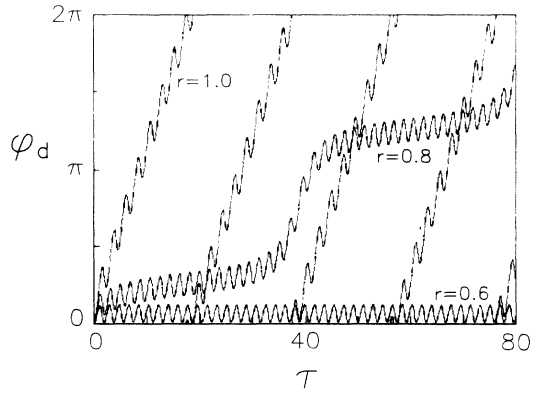


FIG. 4. The angular position $\phi_d$ vs time $\tau$ for two bound spheres in an anisotropic rotating field for different field anisotropy $r$. The angular frequency is the same in all three cases, $\omega'_H = 1.7$. The case $r$=1.0 represents the $M_2^c$ mode , the $r$=0.8 case is a typical example of the $M_2$ mode, while the $r$=0.6 case is an $M_3$ mode as explained in the text.

## IV. NUMERICAL SIMULATIONS

### A. Bound spheres in a circular field

Experimental observations reveal that in the case of bound spheres there exist two distinctly different steady-state modes of motion denoted above by $M_1^c$ and $M_2^c$. In the $M_1^c$ mode observed below a critical frequency $\omega'_H = \omega_1 = 1$ ($\omega_H = \omega_C$), the spheres rotate uniformly with the same angular frequency as the field. Above $\omega'_H = 1$ the $M_2^c$ mode appears. Qualitatively, it can be described as a periodic sequence of forward and backward rotations. In the phase-locked $M_1^c$-mode there develops a constant phase lag $\theta^0 = \phi_H(\tau) - \phi_d(\tau)$ between the direction of the field and the axis through the centers of the spheres. Setting $d\theta/d\tau = 0$ and using Eq. (10) the magnitude of the phase lag is found to be

$$\theta^0(\omega'_H) = \tfrac{1}{2} \arcsin(\omega'_H) \ . \tag{12}$$

The numerical solutions for the $M_2^c$ mode are shown in Fig. 3 where the forward-backward motion relative to the field rotation is clearly seen. The backward motion intervals occur when the phase lag $\theta$ mod $(\pi)$ crosses the value $\pi/2$. At this point the magnetic torque changes sign, reversing the direction of rotation for the pair. This lasts as long as $\theta$ mod $(\pi) \in (\pi/2, \pi)$. The cycle ends when the field and pair axis coincide and the torque direction changes once more.

It is possible to find the angular frequency $\omega_b$ of the backward rotation by integrating Eq. (10) from the end of one backward rotation to the end of the next (for $D$=1 and $r$=1)

$$\omega_b = 2\pi \Big/ \int_0^\pi d\theta \frac{1}{\omega'_H - \sin 2\theta} = 2\sqrt{(\omega'_H)^2 - 1} \ . \tag{13}$$

Since in one period of the forward-backward $M_2^c$ mode the rotating pair loses an angle $\pi$ relative to the rotating field, the average angular velocity of the rotation $\overline{\omega}$ may be expressed as $\overline{\omega} = \omega'_H - \omega_b/2$. Thus we obtain

$$\overline{\omega} = \omega'_H - \sqrt{(\omega'_H)^2 - 1} \tag{14}$$

as the average angular velocity in this case. This curve is shown in Fig. 2. This analytical result was used as a test for the numerical accuracy of our simulations. For $\omega'_H \to \infty$, Eq. (14) gives $\overline{\omega} \approx 1/2\omega'_H$ which is in close agreement with experimental observations. In the other limit $\omega'_H \to 1$,

$$\omega'_H - \overline{\omega} \sim (\omega'_H - 1)^{1/2} = (\omega'_H - \omega_1)^{1/2} \ . \tag{15}$$

Thus $\Delta\overline{\omega} \sim (\Delta\omega'_H)^{1/2}$ and the "critical exponent" for the transition is $\frac{1}{2}$.

### B. Bound spheres in an elliptical field

For an elliptical field, the $M_1$ and $M_2$ modes both change character as seen in Fig. 4. The new $M_1$ and $M_2$ modes are modulated versions of the $M_1^c$ and $M_2^c$ modes.

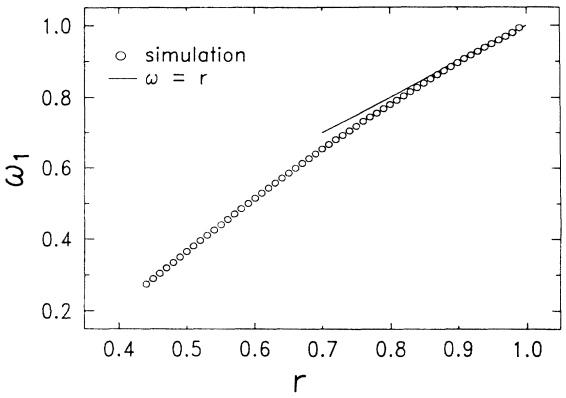


FIG. 5. The values of the lower critical angular frequency $\omega_1$ calculated from simulations for different values of the anisotropy parameter $r$. The solid curve shows the asymptotic behavior for $r \to 1$.

In spite of the modulation, the average frequency of rotation is still $\bar{\omega} = \omega'_H$ in the $M_1$ mode, and as $r \to 1$ the $M_1$ mode changes smoothly into the $M_1^c$ mode. The transition between the $M_1$ and $M_2$ modes takes place at a frequency $\omega_1$ smaller than $\omega_1(r = 1) = 1$. As is shown in Fig. 2, the average angular velocity $\bar{\omega}$ in the $M_2$ mode does not approach 0 asymptotically. Instead, there is a finite transition frequency $\omega_2$ above which the spheres do not rotate but perform an oscillation around some fixed axis. The direction of this axis is midway between the largest and smallest axis of the $H$-field ellipse at $\omega'_H = \omega_2$ and approaches the former as $\omega'_H \to \infty$. This mode, which we call $M_3$, can be considered as a limiting case of mode locking to the magnetic field with ratio $\bar{\omega}$:$\omega'_H$=0:1. As $r$ decreases, the $\omega'_H$ range in which the $M_2$ mode is observed decreases and the $M_2$ mode presumably vanishes below a certain $r$ value. By carefully approaching the $\omega_1$ value from below and the $\omega_2$ value from above, it is possible to get good numerical estimates for these values for different values of $r$. Figures 5 and 6 show these numerical estimates together with the analytical limit for $r \to 1$.

In the Appendix we have derived the simplified equation of motion for the angular motion of the bound pair. Introducing $\epsilon = 1 - r$ as the measure of the deviation from circularity this equation reads

$$\frac{d\phi_d}{d\tau} \approx (1-\epsilon)\sin[2(\omega'_H\tau - \phi_d)] - \epsilon\sin(2\phi_d) = G_{\text{circ}}(1-\epsilon) + G_{\text{eff}}(\epsilon, \phi_d) \ . \tag{16}$$

Its interpretation is relatively simple. $G_{\text{circ}}(1-\epsilon)$ is the torque induced by an effective circular field of magnitude $|h| = \sqrt{1-\epsilon}$. $G_{\text{eff}}(\epsilon, \phi_d)$ is the torque stemming from an effective angular energy barrier

$$U_{\text{eff}}(\phi_d) = -\frac{\epsilon}{2}\cos(2\phi_d) \ . \tag{17}$$

Thus the motion of the bound pair in an elliptic field can be viewed as the motion of a pair induced by an effective circular field within a stationary energy barrier.

For a general equation of the form

$$\frac{d\phi}{dt} = A\sin[2(\omega t - \phi)] \ , \tag{18}$$

the critical frequency is $\omega_1 = A$ and similar to Eqs. (13) and (14) the average angular velocity for $\omega \gg \omega_1$ is $\overline{(d\phi/dt)} = A/2\omega$. Using this and Eq. (16), the frequency $\omega_1$ for the transition from the $M_1$ to the $M_2$ mode in the limit $r \to 1$ is found to be

$$\omega_1(r) = 1 - \epsilon = r \ . \tag{19}$$

From Eq. (16) we get an equation for the average motion

$$\bar{\omega} = (1-\epsilon)\{\sin[2(\omega'_H\tau - \phi_d)]\}_{\text{av}} - \epsilon\sin(2\phi_d) = \frac{1-\epsilon}{2\omega'_H} - \epsilon\sin(2\phi_d) \ . \tag{20}$$

When the average motion vanishes, $\bar{\omega} = 0$, then

$$\omega'_H = \frac{1-\epsilon}{2\epsilon\sin(2\phi_d)} \geq \frac{1-\epsilon}{2\epsilon} \ . \tag{21}$$

The maximum field angular frequency $\omega_2$ for observation of the $M_2$ mode for $r \to 1$ is therefore

$$\omega_2(r) = \frac{1-\epsilon}{2\epsilon} = \frac{r}{2(1-r)} \ . \tag{22}$$

Good empirical fits to the numerical estimates of the critical frequencies for the range $0.5 < r \leq 1.0$ shown in Figs. 5 and 6 are given by

$$\omega_1(r) \approx 2r - \frac{r^2+1}{2} \tag{23}$$

and

$$\omega_2(r) \approx \frac{r}{(1-r)(3-r)} \tag{24}$$

and have the same asymptotic form as the analytical results given above for $r \to 1$. The experimental values of $\omega_1$ and $\omega_2$ (Fig. 2) agree well with the simulations except for $\omega_2$ close to $r$=1 where small experimental deviations from the nominal $r$ value produce large changes in $\omega_2$. The simulations show (Fig. 7) that close to $\omega_1$

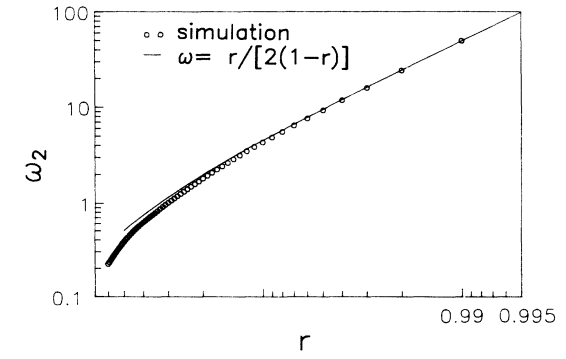


FIG. 6. The solid curve shows the asymptotic behavior $r \to 1$ for the upper critical frequency $\omega_2$, while the circles represent the values found in simulations.

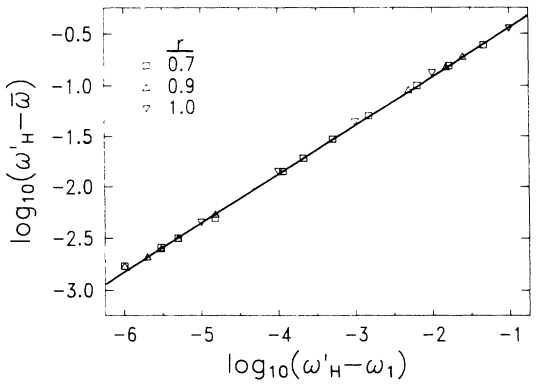


FIG. 7. Plot of $\Delta\bar{\omega} = \omega'_H - \bar{\omega}$ as $\omega'_H \to \omega_1$ calculated by simulations for different field anisotropies $r$. The solid line is the best fit to the data points, and the slope is $0.48 \pm 0.03$.

$$\Delta\bar{\omega} = (\omega'_H - \bar{\omega}) \sim (\Delta\omega'_H)^{0.48\pm0.03} \tag{25}$$

over at least four orders of magnitude, where $\Delta\omega'_H = (\omega'_H - \omega_1)$. This is in close agreement with what was found analytically in the circular $r$=1 case.

### C. Free spheres in a circular field

As long as $\omega'_H$ is small enough, the pair follows the magnetic field since in this mode, $M_1^c$, the lag angle $\theta$ cannot exceed $\pi/4$ [Eq. (12)]. The radial magnetic force $F_d^H$ is then always negative and the pair is bound together by magnetic forces. Above a critical frequency, the situation changes dramatically and a new mode $M_4^c$ appears. The angular motion is similar to the case for bound spheres, but the spheres additionally perform an oscillatory radial motion. The cause for this is simple: Each time $[1 - 3\cos^2(\phi_H - \phi_d)] > 0$, i.e., when $|\phi_H - \phi_d| \bmod (\pi) > 54.7°$, the radial force $F_d^H$ becomes positive and the spheres are pushed apart. Calculating the average speed of rotation $\bar{\omega}$ in this case [Fig. 8(a)], we find that it is larger than it was in the case of bound spheres (Fig. 2). Still, however, as $\omega'_H \to \infty$, $\bar{\omega} \to 0$ asymptotically as in the case for bound spheres.

The experimental data for the nominal $r$=1 case [Fig. 8(b)] show mode locking with ratio $\bar{\omega}$:$\omega'_H$=1:2. The most probable explanation for this somewhat unexpected result is that it is not possible experimentally to produce a perfectly circular symmetry. Even small anisotropies (< 5% for the present system) will break the symmetry and allow mode locking.

Another distinct difference between experiments and simulations was apparent. From the experiments, it was easily observed that the absolute value of the speed was almost constant when the spheres moved through a loop. On the other hand, the simulations gave a dramatic increase in radial velocity when the spheres moved toward each other compared with when they moved away. In addition, the maximum separation found experimentally for $\omega'_H$ near 1 was typically 1.6$a$ (center to center), but only 1.25$a$ was found in the simulations. Thus the radial

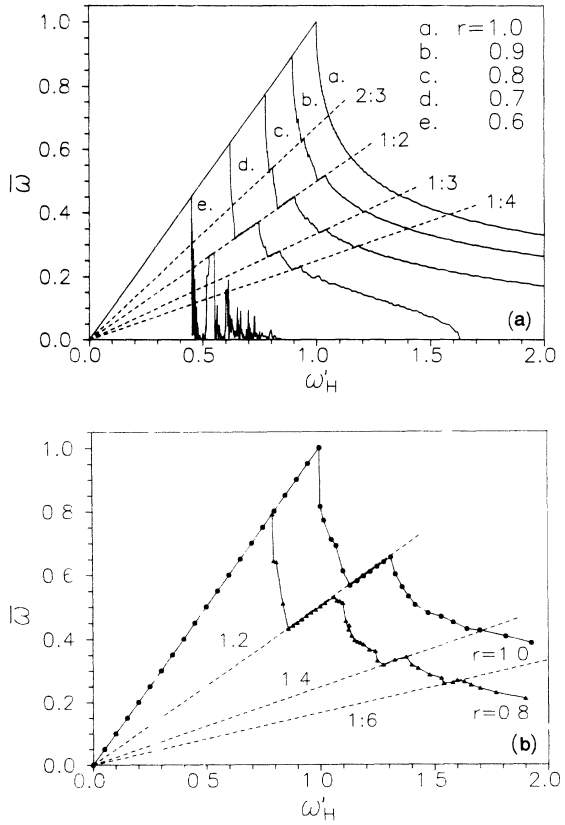


FIG. 8. Plots of the average angular frequency $\bar{\omega}$ vs field angular frequency $\omega'_H$ for two free spheres. (a) The results from the simulations for different field amplitude ratios $r$. (b) The experimental results in two cases. The dashed lines show some of the mode-locked $\bar{\omega}$:$\omega'_H$ ratios.

component of the viscous damping should be decreased and an additional damping term for small sphere separations and approaching spheres should be introduced. The simplest way to do this was by introducing a radial damping factor $K$ on the left-hand side of Eq. (9). Expanding $K$ in powers of sphere separation $D$ and keeping terms up to second order we used

$$K = \begin{cases} A(D - D_0)^2 + B & \text{for } dD/d\tau < 0 \\ \quad \text{and } D < D_0 & \\ B & \text{otherwise} \end{cases} \tag{26}$$

where $A$, $D_0$, and $B$ are constants. For $\omega'_H \approx \omega_1$ reasonable agreement with experiments was found for $A \approx 4$, $D_0 \approx 1.5$, and $B \approx 0.1$. Due to this change, the average $\bar{\omega}$ from the simulations decreased slightly relative to the $K$=1 case for $\omega'_H \gg \omega_1$. $\bar{\omega}$ approached the bound sphere values for $B \to \infty$. However, due to the minor differences thus obtained, we prefer to use the results from the simulations without this damping factor in the following discussions and in all the figures except Figs. 9 and 10.

### D. Free spheres in an elliptical field

Here, the situation is similar to the bound sphere case discussed above. The mode $M_4$ for $r < 1$ changes

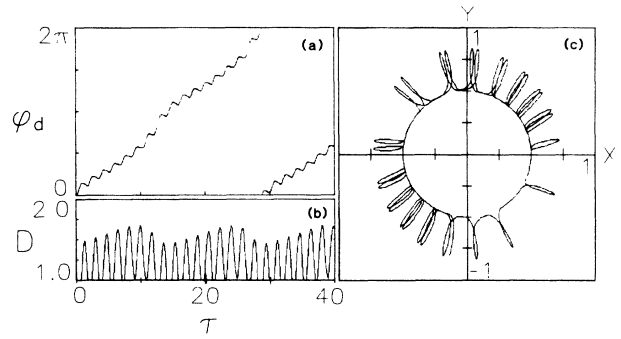


FIG. 9. Sphere motion for a system of two free spheres in an anisotropic rotating field with $r$=0.8 and $\omega'_H$=2.0. This is an example of a typical $M_4$ mode. (a) shows the angular position $\phi_d$ vs time and (b) the corresponding center-to-center separation $D = d/a$. (c) The trace of the motion of the center of one of the spheres [note that the trace is for a longer time period than shown in (a) and (b)].

smoothly into the $M_4^c$ mode as $r \to 1$. Typical simulations of the angular and the radial components of the motion of the spheres for anisotropic fields are shown in Figs. 9(a), 9(b), 10(a), and 10(b) and the trace of the overall motion is shown in Figs. 9(c) and 10(c). Both the experiments and the simulations with $r < 1$ show the mode locking $\overline{\omega}$:$\omega'_H$=1:2. But in addition, mode locking is also found for other $\overline{\omega}$:$\omega'_H$ ratios. The simulations for the case $r$=0.8 clearly show mode locking at the ratios 1:2, 1:3, 1:4, and 2:3 as is shown in Fig. 8(a). This can be compared to the experimental measurements in Fig. 8(b).

The width of the mode-locked $\omega'_H$ intervals for fixed $r$ decreases with increasing denominator $n$ in the 1:$n$ locked modes. Thus, to find the mode-locked intervals, very small steps in $\omega'_H$ are needed. The overall appearance of these results has some resemblance to the widely investigated circle map[14,15] in nonlinear dynamics. It is well known that circle maps, for example,

$$x_{n+1} = x_n + 2\pi\Omega + K\sin(x_n)\ , \tag{27}$$

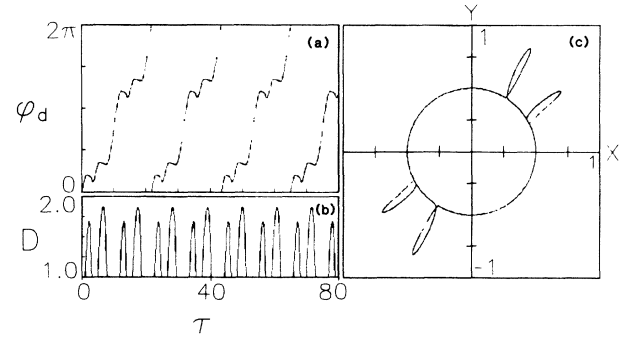


FIG. 10. Same legend as for Fig. 9. In this case $r$=0.7 and $\omega'_H$=0.87. This shows the spheres' motion in the mode-locked $\overline{\omega}$:$\omega'_H$=1:3 state since each time the spheres move through one loop the phase lag $\theta = \phi_H - \phi_d$ is increased by $\pi$. The trace of the motion of one sphere shown in (c) is therefore a closed curve and should be compared to the quasiperiodic motion in Fig. 9(c).

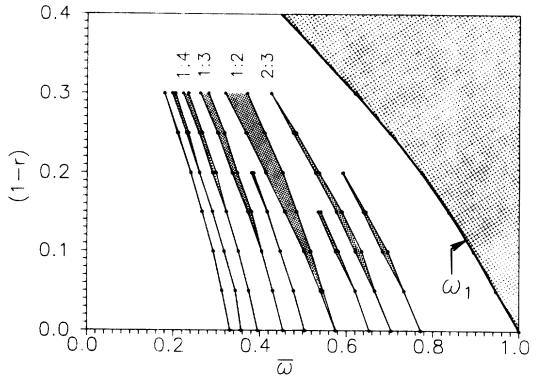


FIG. 11. The shaded areas show the mode-locked intervals (Arnol'd tongues) for different field anisotropy $(1 - r)$ and average pair rotation frequency $\overline{\omega}$ ("winding number"). The crosshatched region is unphysical since $\overline{\omega}(\omega'_H) \leq \overline{\omega}(\omega'_H = \omega_1)$.

show mode locking at every rational winding number $W = 2\pi\Omega$. The width of the mode-locked intervals for the circle map (commonly referred to as Arnol'd tongues) is increasing as the nonlinear coupling constant $K$ is increased. This can be compared to Fig. 11 showing the Arnol'd tongues for different values of the anisotropy parameter $\epsilon = (1 - r)$ in our system. The relation between this case and a particular circle map has not been established at present. Our simulations show that near $r$=0.65 ($\epsilon \approx 0.35$) the motion changes character, and the trajectory in phase space becomes very complicated. As is seen in Fig. 8(a) $\overline{\omega}$ fluctuates a lot for $r$=0.6 and is strongly dependent on the time interval for averaging.

The experimental $r$=0.8 curve in Fig. 8(b) shows that the width of the mode-locked states is larger in the experiments than in the simulations. The $\overline{\omega}$:$\omega'_H$=1:2 locked state dominates and the 1:3 mode is not experimentally observed even though the 1:4 mode is easily obtained. As $\omega'_H \to \infty$, $\overline{\omega}$ goes to zero at a finite but somewhat greater $\omega'_H$ value than the numerical one. Even though the quantitative agreement between the experiments and the simulations is not too good, we believe that the qualitative agreement is reasonable considering the simple model used.

## V. NONPLANAR MAGNETIC FIELDS

In all the cases discussed above the attractive interaction between the spheres has been the dominating one since the spheres are in direct contact for a large part of the time. It is possible to weaken this dominating attraction by introducing an additional constant repulsive potential between the spheres. This can be done by applying a magnetic field $H_\perp$ normal to the sample plane in addition to the circular rotating field $H_\parallel$ in the plane. The magnetic-field vector in the ferrofluid is then rotating on a cone with a cone angle $\alpha$ ($\tan\alpha = H_\parallel/H_\perp$). Depending on the ratio $H_\perp/H_\parallel$ and the field angular frequency $\omega'_H$ three main types of behavior were observed: (i) stable rotation with spheres in contact (mode $M_1^c$), (ii) motion in loops around the mass center with spheres in contact

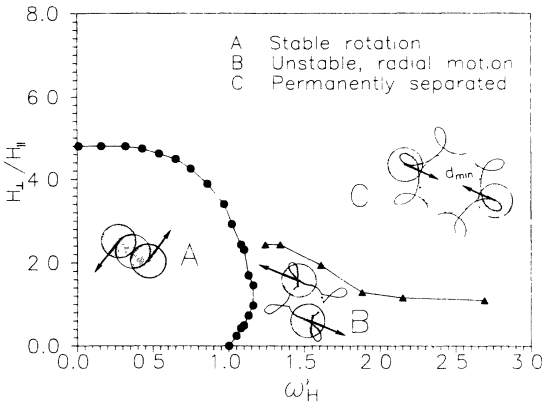


FIG. 12. "Phase" diagram for two free magnetic holes in a rotating field $H_\parallel$ in the plane of motion and with a constant field $H_\perp$ perpendicular to the plane of motion. The angular frequency of the rotating field is $\omega'_H$. The regions for three different modes of motion are marked by $A$, $B$, and $C$ ($A$ and $B$ correspond to the $M_1^c$ and $M_4^c$ modes discussed in the text for $H_\perp=0$, $C$ is the $M_5^c$ mode). The dots represent the $\omega'_H$ value ($=\omega_1$) and $H_\perp/H_\parallel$ ratio at transition from stable rotation to motion in radial loops. Triangles show the transition from the $M_4^c$ mode with spheres in contact part of the time ($d_{min} = a$) to the $M_5^c$ mode with spheres permanently separated ($d_{min} > a$).

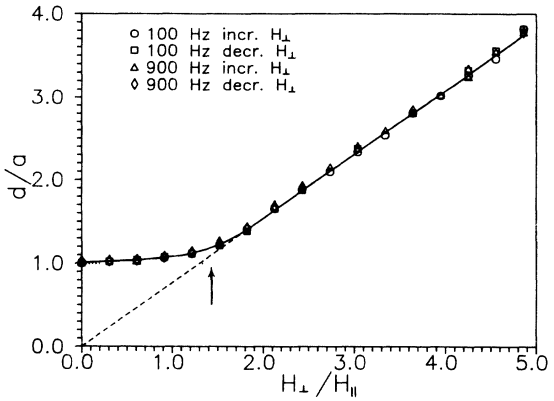


FIG. 13. Center-to-center distance $D = d/a$ for two spheres vs the ratio between the normal field $H_\perp$ and the amplitude $H_\parallel$ of the high-frequency rotating field. This corresponds to plotting $d_{min}$ as the system moves along a vertical line at high $\omega'_H$ in the "phase" diagram in Fig. 12. The slope of the straight line fitting the curve for $d/a > 1.6$ is 0.78. The vertical arrow indicates the theoretical value (dipole model) of $H_\perp/H_\parallel$ at the transition from an average attractive force (left) to an average repulsive force (right) between the spheres.

part of the time (mode $M_4^c$), and (iii) motion in loops with minimum particle separation $d_{min} > a$ (mode $M_5^c$).

Cases (i) and (ii) are the sphere hard-core case discussed previously, while (iii) is similar to spheres with a soft repulsive core with diameter $a_{eff} > a$. No stable rotation mode with separated spheres was observed. The "phase" diagram for these rotation modes is shown in Fig. 12. At low $\omega'_H$ and small ratio $H_\perp/H_\parallel$ the $M_1^c$ mode is the preferred one. As $\omega'_H$ increases the system passes into either the $M_4^c$ or the $M_5^c$ mode (denoted $B$ and $C$ in Fig. 12) depending on $H_\perp/H_\parallel$. For $H_\perp/H_\parallel > 5$ the $M_5^c$ mode is the only stable one for all frequencies. This is easy to understand as the cone angle $\alpha < 11°$ and the magnetic moments of the spheres are almost perpendicular to the line between the centers of the spheres. The magnetic force between the spheres is then repulsive.

The most interesting property of this phase diagram is the behavior near $\omega'_H = 1$ and $H_\perp/H_\parallel \approx 0$. The experiments show that a small $H_\perp$ tends to stabilize the $M_1^c$ mode and then the transition frequency $\omega_1$ increases with increasing $H_\perp$. This continues until $H_\perp/H_\parallel$ is between 1.2 and 1.5. At this point the cone angle is close to the value where the magnetic dipole force $F_d^H \sim \{1-3\cos^2[(\pi/2)-\alpha]\}$ changes sign from attractive to repulsive. Above this $H_\perp$ value, the stability range of the $M_4^c$ mode grows at the expense of the $M_1^c$ mode and $\omega_1$ decreases. For $H_\perp/H_\parallel > 2.5$ the $M_5^c$ mode is the most stable at high frequencies, but the transition between the $M_4^c$ and the $M_5^c$ mode is difficult to observe due to the long relaxation time. The effective (average) sphere separation in the $M_5^c$ mode increases with increasing $H_\perp$, and the size of the loops decreases as $\omega'_H$ increases. Most of the observed behavior can be understood qualitatively from simple arguments based on the dipole model of the interactions.

The phase diagram indicates the possibility of obtaining a fixed but tunable separation between the spheres by going to high $\omega'_H$ values where the size of the loops in the $M_5^c$ mode vanishes. In fact, it is possible to adjust the distance between the spheres continously from contact to any fixed separation by varying the $H_\perp/H_\parallel$ ratio at high $\omega'_H$ (typically, $\omega'_H = 10 - 100$).

The separation grows linearly with $H_\perp$ above a threshold value $H_\perp/H_\parallel \approx 1.6$ (Fig. 13), and can be approximated by

$$\frac{d}{a} = 0.78\frac{H_\perp}{H_\parallel} . \tag{28}$$

There is no difference between increasing and decreasing field (no hysteresis). The experiments were repeated for different frequencies from 20 Hz up to 1 kHz and exactly the same behavior was observed. These observations contradict our simple dipole model which predicts that the spheres should stay together for $H_\perp/H_\parallel < 1.4$ (marked by an arrow in Fig. 13) and should become infinitely separated above this value.

## VI. CONCLUSIONS

The results of our studies of very simple systems of magnetic holes in external rotating magnetic fields show that the dynamics of the system is complicated, but can in the simplest cases be well described by an overdamped nonlinear equation of motion including magnetic dipole forces and viscous forces. Several basically different modes of motion were observed, depending on the

frequency of the rotating magnetic field, the anisotropy of the $H$ field, and the magnitude of added constant fields normal to the plane of motion. Increasing anisotropy in the rotating field ($r < 1$) tends to destabilize the low-frequency stable rotation $M_1$ mode and force the system into oscillations around a fixed axis (the $M_3$ mode).

The simplest case with spheres bound together showed good agreement between the numerical simulations and the experiments. For spheres with radial motion, there was qualitative agreement between simulations based on our simple dipole model and the experiments, even though the quantitative agreement was less good. The average rotation of the system showed mode locking to the external rotating magnetic field in certain frequency intervals.

It seems worth noting that for the case of bound spheres in a circular field (i.e., $D$=1 and $h$=1) Eq. (10) can be easily transformed to the reference frame of the rotating magnetic field where it takes the form of the equation of motion of an overdamped pendulum under a constant torque. This simple system has been shown to model well a particular case of a Josephson junction.[16] It is quite possible that in view of this analogy some of the results we presented can be of use in analysis of experiments performed on the latter system.

The introduction of a constant field $H_\perp$ perpendicular to the plane of rotation stabilized the $M_1$ mode for small $H_\perp/H_\parallel$. Three different modes of motion were possible: (i) stable rotation (small $H_\perp/H_\parallel$ and small $\omega'_H$), (ii) motion in loops around the center of the system with spheres in contact part of the time (small $H_\perp/H_\parallel$, large $\omega'_H$), or (iii) permanently separated spheres (large $H_\perp/H_\parallel$). At high frequencies the motion vanished and the spheres stabilized at a fixed separation.

As the important feature of our model is the difference $\Delta\mu$ between the magnetic permeability $\mu_p$ of the spheres (holes) and that of the surrounding medium $\mu_s$, it should be possible to observe the same phenomena in systems consisting of paramagnetic particles in a nonmagnetic liquid (water). In fact, we have done similar experiments using superparamagnetic spheres[10] of the same size dispersed in a water-sugar solution with almost the same viscosity as the ferrofluid and observed the same behavior as for magnetic holes. Preliminary experiments with paramagnetic spheres having a fixed remanent magnetization showed similar behavior except that in this case the spheres had an internal "spin" degree of freedom. This gave rise to an additional rotation of each individual sphere about its center in the same direction as the field. The observed behavior could be reproduced numerically using a model similar to Eqs. (1)–(7) with added terms taking care of the interaction between the permanent magnetic moments and the external field.

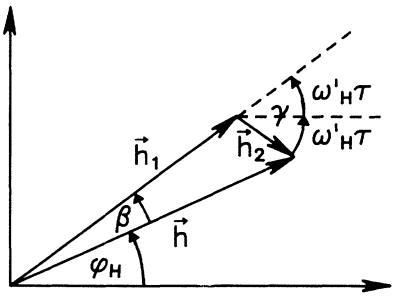


FIG. 14. The decomposition of the rotating field h into two components, $\mathbf{h}_1$ and $\mathbf{h}_2$, rotating in opposite directions with angular velocity $\omega'_H$.

## ACKNOWLEDGMENTS

This research was supported in part by Dyno Industrier A.S. and by the Norwegian Research Council for Science and the Humanities (NAVF). One of us (P.P.) wants to acknowledge the support from NAVF during a stay at the Institute for Energy Technology, Kjeller. We would like to thank J. Ugelstad, A. Berge, and T. Ellingsen for supplying the spheres used in the experiments and J.L. McCauley, J.P. Hansen, and Z.J. Yang for valuable discussions.

## APPENDIX

To derive a simplified equation of motion for the bound pair of spheres we start from Eq. (10) with $D$=1

$$\frac{d\phi_d}{d\tau} = h^2 \sin[2(\phi_H - \phi_d)] \,. \tag{A1}$$

Introducing $\epsilon = 1 - r$ for the deviation from circularity, using the trigonometric relation $\cos(2\omega'_H\tau) = 1 - 2\sin^2\omega'_H\tau$, and keeping terms to first order in $\epsilon$, Eq. (11) can be rewritten as

$$\begin{aligned} h^2 &= \cos^2(\omega'_H\tau) + (1-\epsilon)^2 \sin^2(\omega'_H\tau) \\ &\approx (1-\epsilon) + \epsilon\cos(2\omega'_H\tau) \,. \end{aligned} \tag{A2}$$

Combining Eqs. (A1) and (A2) we get

$$\begin{aligned} \frac{d\phi_d}{d\tau} &= (1-\epsilon)\sin[2(\phi_H - \phi_d)] \\ &\quad + \epsilon\cos(2\omega'_H\tau)\sin[2(\phi_H - \phi_d)] \,. \end{aligned} \tag{A3}$$

To further simplify Eq. (A3) we need a simple expression for the angle $\phi_H$. The dimensionless field $\mathbf{h} = \mathbf{H}/H_0$ can be decomposed into two parts $\mathbf{h}_1$ and $\mathbf{h}_2$:

$$\begin{aligned} \mathbf{h}(\tau) &= \cos(\omega'_H\tau)\,\mathbf{i} + (1-\epsilon)\sin(\omega'_H\tau)\,\mathbf{j} \\ &= (1 - \tfrac{1}{2}\epsilon + \tfrac{1}{2}\epsilon)\cos(\omega'_H\tau)\,\mathbf{i} + (1 - \tfrac{1}{2}\epsilon - \tfrac{1}{2}\epsilon)\sin(\omega'_H\tau)\,\mathbf{j} \\ &= (1 - \tfrac{1}{2}\epsilon)[\cos(\omega'_H\tau)\,\mathbf{i} + \sin(\omega'_H\tau)\,\mathbf{j}] + \tfrac{1}{2}\epsilon[\cos(\omega'_H\tau)\,\mathbf{i} - \sin(\omega'_H\tau)\,\mathbf{j}] \\ &= \mathbf{h}_1 + \mathbf{h}_2 \,. \end{aligned} \tag{A4}$$

The field $\mathbf{h}_1$ of magnitude $h_1 = |\mathbf{h}_1| = (1 - \frac{1}{2}\epsilon)$ rotates in the counterclockwise direction with angular frequency $\omega'_H$ and the field $\mathbf{h}_2$ of magnitude $h_2 = |\mathbf{h}_2| = \frac{1}{2}\epsilon \ll h_1$ rotates in the opposite or clockwise direction. The angle $\gamma$ between these two vectors (Fig. 14) is $\gamma = 2\omega'_H\tau \bmod (2\pi)$. Let us denote the angle between $\mathbf{h}$ and $\mathbf{h}_1$ by $\beta$. From Fig. 14 it is seen that $\phi_H = \omega'_H\tau - \beta$. Using the general sine rule for a triangle we get $\sin\beta = [\sin(\pi - \gamma)](h_2/h) \approx (\sin\gamma)h_2/h_1$. Since $h_2 \ll h$, $\beta$ is a very small angle and $\sin\beta$ can be replaced by $\beta$. Thus $\beta$ can be approximated by

$$\beta \approx \sin(2\omega'_H\tau)\tfrac{1}{2}\epsilon/(1 - \tfrac{1}{2}\epsilon) \approx \frac{\epsilon}{2}\sin(2\omega'_H\tau) \qquad \text{(A5)}$$

and then

$$\phi_H \approx \omega'_H\tau - \frac{\epsilon}{2}\sin(2\omega'_H\tau)\ . \qquad \text{(A6)}$$

Substituting Eq. (A6) for $\phi_H$ into Eq. (A3) and keeping terms to first order in $\epsilon$, we get a first-order approximation for the equation of motion:

$$\begin{aligned}\frac{d\phi_d}{d\tau} &\approx (1-\epsilon)\sin\{2[\omega'_H\tau - \tfrac{1}{2}\epsilon\sin(2\omega'_H\tau) - \phi_d]\} + \epsilon\cos(2\omega'_H\tau)\sin[2(\omega'_H\tau - \phi_d)] \\ &= (1-\epsilon)\sin[2(\omega'_H\tau - \phi_d)] - \epsilon\cos[2(\omega'_H\tau - \phi_d)]\sin(2\omega'_H\tau) + \epsilon\sin[2(\omega'_H\tau - \phi_d)]\cos(2\omega'_H\tau) \\ &= (1-\epsilon)\sin[2(\omega'_H\tau - \phi_d)] + \epsilon\sin[2(\omega'_H\tau - \phi_d) - 2\omega'_H\tau] \\ &= (1-\epsilon)\sin[2(\omega'_H\tau - \phi_d)] - \epsilon\sin(2\phi_d)\ . \end{aligned} \qquad \text{(A7)}$$

This is the same as Eq. (16).


[1] A.T. Skjeltorp, Phys. Rev. Lett. **51**, 2306 (1983).

[2] A.T. Skjeltorp, J. Magn. Magn. Mat. **65**, 195 (1987).

[3] M. Warner and R.M. Hornreich, J. Phys. **A 18**, 2325 (1985). Some of the conclusions drawn in this theoretical paper are not consistent with experimental observations. For example, it has been predicted that there could be possible transformations from a planar triangular to a quadratic lattice or to an out-of-plane three-sublattice triangular ordering as the layer thickness increases. What is observed instead are transformations to, e.g., honeycomb lattices with up-down ordering of touching spheres.

[4] A.R. Laufer, Am. J. Phys. **19**, 275 (1951).

[5] J.J. Newman and R.B. Yarbrough, J. Appl. Phys. **39**, 5566 (1968).

[6] R.W. Chantrell and E.P. Wohlfart, J. Magn. Magn. Mat. **40**, 1 (1983).

[7] R.E. Rosensweig, Annu. Rev. Fluid Mech. **19**, 437 (1987).

[8] For cell separation and immunological analysis, see A. Berge, T. Ellingsen, K. Nustad, S. Funderud, and J. Ugelstad, in *Scientific Methods for the Study of Polymer Colloids and Their Applications*, edited by F. Candau and R.H. Ottewill (Kluwer, Dordrecht, 1989), p. 517.

[9] Type EMG 909 from Ferrofluidics Corp. with saturation magnetization $M_s$=200 G, initial susceptibility $\chi$=0.0829, and viscosity $\eta$=5 cP.

[10] J. Ugelstad *et al.*, Adv. Colloid Interface Sci. **13**, 101 (1980). Produced under the trade name Dynospheres by Dyno Particles A.S., N-2001 Lillestrøm, Norway.

[11] In the sample preparation it was found that most spheres brought together by external fields and kept in contact for some time stayed permanently together. The mechanism for this is not known.

[12] G. Helgesen, P. Pieranski, and A.T. Skjeltorp, Phys. Rev. Lett. **64**, 1425 (1990).

[13] There are image dipole effects across the cell boundaries, Ref. 3. For the present experimental realization, the image dipole contribution is relatively small (typically $\leq$ 10%) compared to the interaction energy between the real dipoles. There are also image dipole effects from one sphere onto the other. See, e.g., D. Bedeaux, M.M. Wind, and M.A. van Dijk, Z. Phys. B **68**, 343 (1987). This contribution is also small ($\approx$ 6% for $D$=1.1) and may be neglected in the present analysis.

[14] H.G. Schuster, *Deterministic Chaos* (VCH Verlag, Weinheim, 1988).

[15] J.L. McCauley, Phys. Scr. **20**, 1 (1988).

[16] D.B. Sullivan and J.E. Zimmerman, Am. J. Phys. **39**, 1504 (1971).

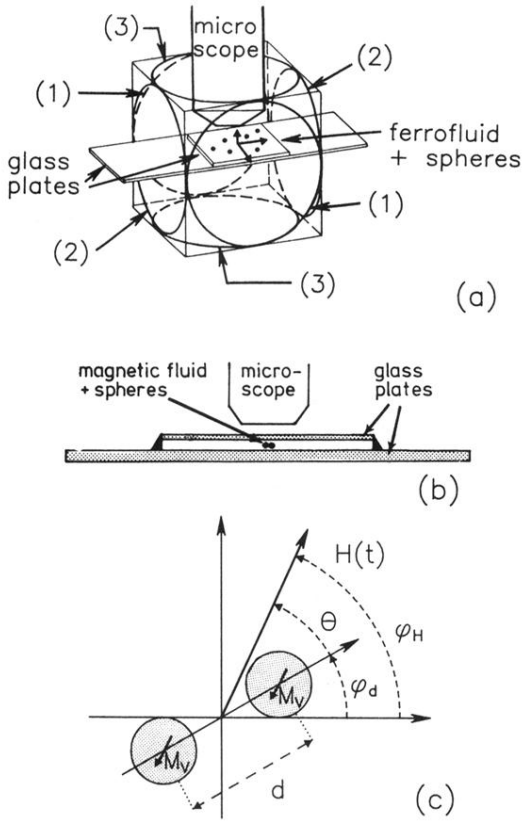


FIG. 1. (a) Experimental setup, showing the three orthogonal pairs of coils labeled (1), (2), and (3). (b) Side view of experimental setup (without coils). (c) Top view, coordinate system for two magnetic holes rotating in the plane between the glass plates in (b).

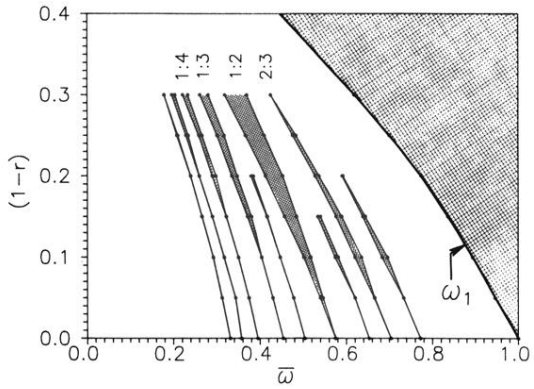


FIG. 11. The shaded areas show the mode-locked intervals (Arnol'd tongues) for different field anisotropy $(1 - r)$ and average pair rotation frequency $\overline{\omega}$ ("winding number"). The crosshatched region is unphysical since $\overline{\omega}(\omega'_H) \leq \overline{\omega}(\omega'_H = \omega_1)$.

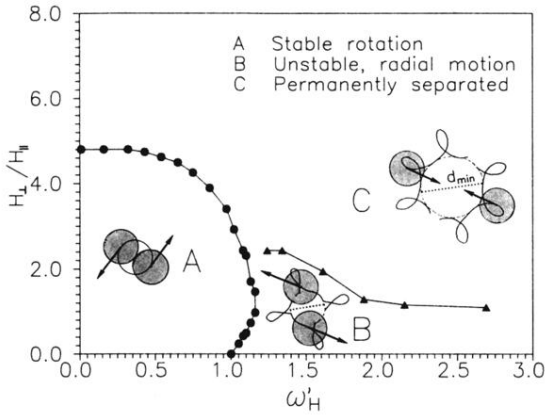


FIG. 12. "Phase" diagram for two free magnetic holes in a rotating field $H_\parallel$ in the plane of motion and with a constant field $H_\perp$ perpendicular to the plane of motion. The angular frequency of the rotating field is $\omega'_H$. The regions for three different modes of motion are marked by $A$, $B$, and $C$ ($A$ and $B$ correspond to the $M_1^c$ and $M_4^c$ modes discussed in the text for $H_\perp$=0, $C$ is the $M_5^c$ mode). The dots represent the $\omega'_H$ value (=$\omega_1$) and $H_\perp/H_\parallel$ ratio at transition from stable rotation to motion in radial loops. Triangles show the transition from the $M_4^c$ mode with spheres in contact part of the time ($d_{\min} = a$) to the $M_5^c$ mode with spheres permanently separated ($d_{\min} > a$).